CFD Prediction of Slot Jet Impingement Heat Transfer

Rossella D'Addio(✉), Antonio Mezzacapo, and Giuliano De Stefano

Engineering Department, University of Campania Luigi Vanvitelli, 81031 Aversa, Italy
rossella.daddio@unicampania.it

Abstract. This work numerically investigates the heat transfer characteristics of a wide-slot jet impinging orthogonally on an isothermal hot plate. The case study consists of an incompressible turbulent jet flow with a Reynolds number of 11000. Two-dimensional Reynolds-averaged Navier–Stokes (RANS) simulations are performed utilizing three different turbulence closures, namely, realizable k-ϵ, k-ω SST, and the recently developed generalized k-ω (GEKO) models. Diagnostics include air flow characteristics, as well as surface pressure and local Nusselt number distributions. The influence of using production limiters to mitigate the excessive generation of turbulent kinetic energy in the stagnation region is addressed by means of detailed comparisons against reference experimental findings. The various models capture the pressure distribution on the plate with good accuracy. As far as classical approaches are concerned, the realizable k-ϵ model significantly overestimates heat transfer due to excessive turbulent diffusion, whereas the k-ω SST model provides much better agreement with experiments. Moreover, the default GEKO parameters are found to inadequately represent the flow physics of the slot jet configuration. To address this limitation, two alternative sets of model coefficients are proposed, which provide better results.

Keywords: Computational fluid dynamics · slot jet impingement · RANS equations · Nusselt number · two-equation eddy-viscosity models · generalized turbulence modeling · production limiters

1 Introduction

Impinging jets are frequently employed in various industrial applications for the purpose of transferring energy and mass. Examples of such applications include the cooling of electronic devices, the utilization of thermal spray jets in manufacturing processes, the operation of launch platforms, the function of jet deflectors, as well as their use in extra-terrestrial landings and in the context of V/STOL (vertical and/or short take-off and landing) aircraft [1]. Nguyen et al. [2] noted that jet flow physics might be influenced by several geometric parameters, namely the diameter of the nozzle exit, the distance from the nozzle to the wall, and the angle of inclination of the plate [3].

© The Author(s), under exclusive license to Springer Nature Switzerland AG 2025
O. Gervasi et al. (Eds.): ICCSA 2025, LNCS 15650, pp. 309–324, 2025.
https://doi.org/10.1007/978-3-031-96962-1_21

On the one hand, the true reproduction of the jet flow physics in experimental studies is very demanding. To analyze the aerodynamic field, several experimental campaigns have been performed, for either supersonic or subsonic jets. For example, Nakai et al. [4] studied the jet flow structures by means of Schlieren images, while Senter and Solliec [5] used the particle image velocimetry (PIV) technique. In addition, experimental measurements of heat transfer have been largely addressed in subsonic jet impingement. For example, Gardon and Akfirat [6] used transducers with high spatial resolution to measure the jet heat transfer characteristics. On the other hand, with the increase of computational power, computational fluid dynamics (CFD) is being largely used to study the eddy structures in turbulent jet flows. For example, Tsubokura et al. [7] performed a numerical study to understand how inlet disturbances may affect the eddy structures, while Hattori and Nagano [8] numerically studied the effects of the impingement distance on the jet heat transfer using direct numerical simulation (DNS). Although DNS data have sometimes been used to evaluate the performance of lower-order turbulence models [9], however, the Reynolds-averaged Navier-Stokes (RANS) approach remains the most widely used to obtain rapid results of engineering interest, e.g. [10]. Several studies with different RANS turbulence models have been performed to assess their capability to reproduce the Nusselt number distribution on the plate. For example, Bovo et al. [11] performed steady-state and transient simulations with different turbulence models. According to their findings, the large-eddy simulation (LES) approach is able to reproduce the turbulent structures with a high degree of accuracy. As far as RANS models are concerned, the k-ϵ model is not sufficiently accurate in predicting heat transfer in the impingement zone, while the k-ω appears more accurate.

In this context, the primary objective of this work is to study the heat transfer characteristics of an impinging slot jet using modern turbulence models. Actually, as standard models have been widely validated, e.g. [12], and their limitations across various flow regimes are well documented, this study focuses on the recently developed generalized k-ω (GEKO) model, including a customized set of parameters. Recently, this model was demonstrated to provide acceptable predictive accuracy for circular jets [13]. Herein, in contrast to conventional circular jet configurations, the wide slot jet setup is chosen for its ability to promote a more uniform heat transfer distribution across the impingement surface, making it particularly suitable for applications requiring consistent thermal management, e.g. [14]. In addition, the influence of Kato-Launder and production limiters, which play a crucial role in predicting the Nusselt number distribution, is investigated. As highlighted by Gurgul et al. [15], RANS models often fail to accurately predict heat transfer due to excessive production of turbulent kinetic energy, especially in the near-wall region. These discrepancies are strongly affected by uncertainties in boundary conditions, turbulence modeling choices, and geometric configurations.

Assessing the ability of modern turbulence models to accurately predict jet impingement heat transfer is crucial for various engineering applications

where stagnation flow regions influence pressure drag and aerodynamic efficiency, affecting fuel consumption and structural integrity. Additionally, in high-speed flows, such as in turbomachinery or spacecraft reentry applications, stagnation flow regions can lead to excessive thermal loads and material erosion. In this applied CFD work, numerical simulations are performed with fixed nozzle-to-plate distance and Reynolds number, and the obtained results are compared with the experimental data available in the literature. The effect of various turbulence models, with and without limiters, is investigated. As all models show good capabilities in predicting the Nusselt number peak and reproducing the experimental trend of velocity and pressure fields, the Nusselt number distribution is approximated with various degrees of accuracy by the different models.

The remainder of the paper is organized as follows. In Sect. 2, the physical model for the jet flow under investigation is introduced, including the mean flow governing equations and the turbulence closures. Section 3 provides the overall computational model, including the numerical settings and the boundary conditions. The main results of the simulations are given and discussed in Sect. 4, while some concluding remarks are offered in Sect. 5.

2 Physical Model

2.1 Case Study

The present applied CFD work investigates the steady incompressible jet flow issuing from a finitely long nozzle with constant section. The reference configuration can be found in the experimental works by either Gardon and Akfirat [6] or Senter and Solliec [5] that were performed with wide slot nozzles. Practically, the case study consists of a two-dimensional air jet impinging orthogonally on an isothermal plate at a fixed distance. Here, the nozzle-to-plate distance is set to $6D_j$, where D_j is the inlet duct diameter, according to reference experimental [6] and numerical [16] works.

The jet flow Reynolds and Mach numbers are defined as follows:

$$Re = \frac{\rho V_j D_j}{\mu}, \tag{1}$$

$$Ma = \frac{V_j}{\sqrt{\gamma R T_j}}, \tag{2}$$

where V_j is the inlet velocity, and T_j stands for the inlet temperature. Due to expected small temperature variations [17], the thermophysical properties of air are considered constant, with the prescribed values summarized in Table 1. Therefore, given and known the inlet conditions provided in Table 2, the above two flow parameters take the values $Re = 11000$ and $Ma = 0.044$, respectively.

The turbulent jet impingement heat transfer is analyzed in terms of local Nusselt number distribution along the cooled wall. This non-dimensional parameter is defined as follows:

$$Nu = \frac{\dot{q} D_j}{\lambda (T_w - T_j)}, \tag{3}$$

Table 1. Constant thermophysical properties of air.

Density ρ, kg/m^3	Heat Capacity C_p, J/(kg·K)	Thermal Conductivity λ, W/(m·K)	Dynamic Viscosity μ, Pa·s
1.225	1006.43	0.0242	1.7894×10^{-5}

Table 2. Inlet boundary conditions.

Boundary type	Values
Velocity inlet	$V_j = 16.25\,\mathrm{m/s}$; $T_j = 338\,\mathrm{K}$; 9% turbulent intensity

where $\dot{q}$ is the heat transfer, with λ representing the thermal conductivity.

The pressure distribution on the plate and the heat transfer coefficient predicted by the present numerical calculations are compared against the experimental data in [6], obtained for the same nozzle-to-plate distance of $6D_j$ at the same Reynolds number. In addition, the mean velocity profiles are compared with the corresponding experimental findings in [5], which were observed for a nozzle-to-plate distance of $8D_j$ at a slightly different Reynolds number, namely $Re = 10600$.

2.2 Governing Equations

Due to the particular jet configuration under investigation, the mean turbulent flow can be assumed to be two-dimensional. In the steady RANS framework, the mathematical equations governing the mean incompressible jet flow can be written as follows:

$$\frac{\partial U_i}{\partial x_i} = 0, \tag{4}$$

$$\frac{\partial}{\partial x_j}(U_i U_j) = -\frac{1}{\rho}\frac{\partial P}{\partial x_i} + \frac{\partial}{\partial x_j}\left(2\nu S_{ij} - \overline{u_i' u_j'}\right), \tag{5}$$

$$\frac{\partial}{\partial x_i}(U_i \Theta) = \frac{\partial}{\partial x_i}\left(a\frac{\partial \Theta}{\partial x_i} - \overline{u_i' \Theta'}\right). \tag{6}$$

They represent the resolved transport equations for mass, momentum, and energy, respectively. In the above equations: U_i $(i = 1, 2)$ correspond to (U,V) that are the mean velocity components; P is the mean pressure; Θ is the mean temperature. Moreover, ρ and ν are the constant density and kinematic viscosity of the fluid, while a stands for its thermal diffusivity. The mean strain rate tensor components are given by:

$$S_{ij} = \frac{1}{2}\left(\frac{\partial U_i}{\partial x_j} + \frac{\partial U_j}{\partial x_i}\right). \tag{7}$$

The RANS equations contain unknown terms that are expressed in terms of velocity fluctuations (u_1', u_2') and temperature fluctuations Θ', specifically

Reynolds stresses $\overline{u_i' u_j'}$ and turbulent heat flux components $\overline{u_i' \Theta'}$, which need to be modeled. As such, additional equations are necessary to model the turbulence closure in the mathematical model.

2.3 Turbulence Closure

In the present study, the performances of three different RANS turbulence models are evaluated, namely: realizable k-ϵ, k-ω SST (shear-stress transport) and generalized k- ω (GEKO) models. All these two-equation eddy-viscosity models use the following approximation for the Reynolds stresses:

$$\overline{u_i' u_j'} = -2\nu_t S_{ij}, \tag{8}$$

where ν_t represents the turbulent viscosity that is the model parameter. Two additional equations are solved to determine the eddy viscosity field, corresponding to the transport equations for turbulent kinetic energy (k) and dissipation (ϵ) or specific dissipation ($\omega = \epsilon/k$). These equations, which are not reported here for brevity, can be found, for instance, in [18].

As far as the turbulent heat flux is concerned, the following approximation is used:

$$\overline{u_i' \Theta'} = -a_t \frac{\partial \Theta}{\partial x_i}, \tag{9}$$

where a_t represents the turbulent diffusivity. The latter parameter is determined by relying on the turbulent Prandtl number Pr_t, defined as:

$$Pr_t = \frac{\nu_t}{a_t}, \tag{10}$$

which is assumed constant.

The realizable k-ϵ represents an improved version of the original k-ϵ model, designed to enhance accuracy in flow cases involving strong streamline curvature, vortices and rotational effects. The adjective "realizable" refers to its ability to satisfy the positivity of normal stresses and Schwarz inequality for shear stresses. In particular, Shih et al. [19] improved the eddy viscosity formulation by using a revised dissipation equation, effectively addressing the round jet anomaly observed in the standard k-ϵ model [20]. The k-ω SST model was specifically designed to improve the prediction of flow separation under adverse pressure gradients by incorporating transport effects into the eddy-viscosity formulation.

The GEKO model represents a very recent version of the k-ω model [21]. It features six adjustable coefficients that allow users to fine-tune the modeling procedure without affecting the fundamentals calibrations for basic flows. Among these coefficients, two parameters are intended for wall-bounded flow, other two for free shear flow, one for corner flow simulation, and one for curvature correction, e.g. [22]. The various parameters of GEKO model are summarized in Table 3, together with the associated controlling function, recommended range of variation, and default value. Specifically, the parameters C_{sep} and C_{nw} are defined for wall-bounded flows, while C_{mix} is actually computed from C_{sep};

C_{corner} and C_{curv} are used for the corner flow correction and the curvature correction, respectively, while C_{jet} is a parameter which controls the accurate prediction of jet flows.

Table 3. GEKO model parameters.

Parameter	Controlling	Range	Default
C_{sep}	Separation behavior	0.7–2.5	1.75
C_{nw}	Near wall behavior	−2.0–2.0	0.5
C_{mix}	Spreading rate of free shear flows	0.5–1.0	C_{mix}^{opt}
C_{jet}	Free jet flows	0.0–1.0	0.9
C_{corner}	Corner flows	0.0–1.5	1.0
C_{curv}	Curvature correction	0.0–1.5	1.0

3 Applied CFD Model

3.1 Computational Domain

A schematic view of the two-dimensional computational domain is reported in Fig. 1, where $(x, y) \equiv (x_1, x_2)$ represent the wall-parallel and wall-normal directions, respectively. The spatial extents of the domain are explicitly indicated, with the impacted wall corresponding to $y = 0$, while $x = 0$ coincides with the duct axis. In particular, the rectangular domain extends up to $40D_j$ in the wall-parallel direction to avoid the influence of outlet boundary conditions on the core region of the impinging jet flow. The inlet duct has a length of $20D_j$, in order to ensure a fully developed velocity profile at the exit duct section.

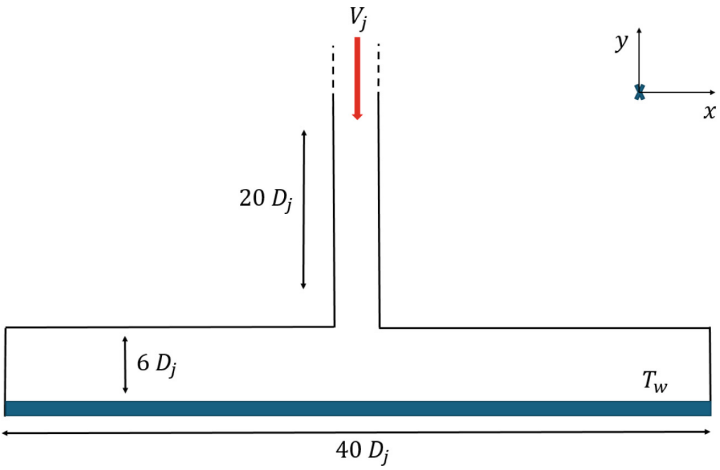


Fig. 1. Schematic view of the computational domain (not in scale).

3.2 CFD Solver

The present numerical simulations are performed by employing the commercial CFD software ANSYS Fluent 2022 R2, which is based on the Finite Volume (FV) approach for incompressible flow, e.g. [23]. The steady RANS governing equations are supplied with suitable boundary conditions. Specifically, the no-slip boundary condition is applied to the solid walls. At the nozzle inlet, a velocity-inlet boundary condition is imposed, while the pressure outlet condition is applied at the outlet boundaries. The outlet and wall boundary conditions are summarized in Table 4.

Due to the incompressible nature of the flow, the SIMPLE algorithm is selected for pressure-velocity coupling, while the gradients are determined using the least squares cell-based method. For the spatial discretization of pressure field, the second-order scheme is chosen. The first-order upwind scheme is used to calculate the momentum, turbulence variables, and energy equation terms. The solution is considered converged when the normalized residual of each variable became less than 10^{-6}.

Table 4. Outlet and wall boundary conditions.

Boundary	Type	Values
Outlet	Pressure outlet, fixed pressure	101325 Pa
Impingement wall	No-slip, fixed temperature	$T_w = 373$ K

3.3 Numerical Mesh

An overview of the numerical mesh is reported in Fig. 2, along with a close-up view in the proximity of the wall impingement zone. The production mesh consists of about forty-two thousand FV cells, with structured elements in the close proximity of the wall, and triangular elements away from the plate. The meshing strategy enables a gradual transition from structured to unstructured mesh elements, effectively reducing the overall computational complexity of the CFD model. Special attention is paid to the height of the first computational cell in the wall-normal direction, which is maintained at the order of $0.01D_j$, which ensures $y^+ \approx 1$.

To address the spatial grid dependence, a mesh convergence study was conducted using the GEKO model, without any limiters. Three different spatial resolutions were employed, namely using 30k (Grid I), 42k (Grid II), and 52k (Grid III) computational cells. The corresponding distributions of Nusselt number are shown in Fig. 3. The medium grid is considered suitable for this work, and was used to generate the results presented in Sect. 4.

4 Results and Discussion

The results of the present simulations allow to assess the capability of the novel GEKO model for incompressible impinging jet flow. Differently from both realizable k-ϵ and k-ω SST models, representing classical approaches to turbulent flow simulation, the modern GEKO model enables fine-tuning and optimal adjusting of the turbulence closure through free model coefficients, e.g. [22]. The default values of GEKO model coefficients, namely those reported on the last column of Table 3, are initially used for the current CFD analysis. Notably, the terms

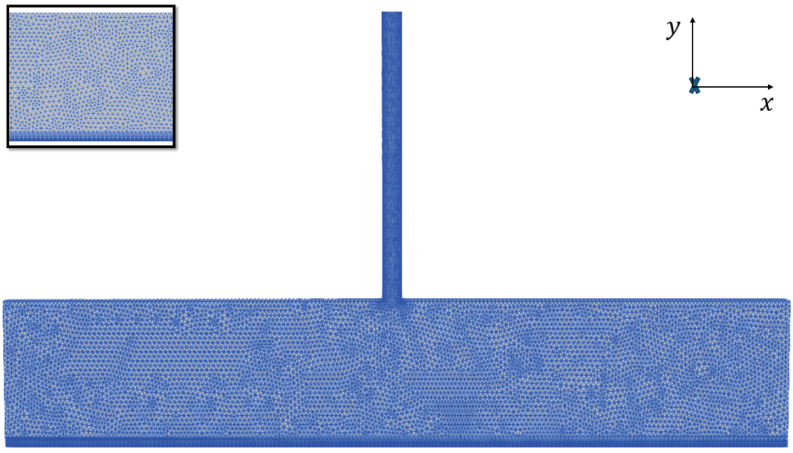


Fig. 2. Sketch of the computational grid, with zoomed-in picture of the wall region.

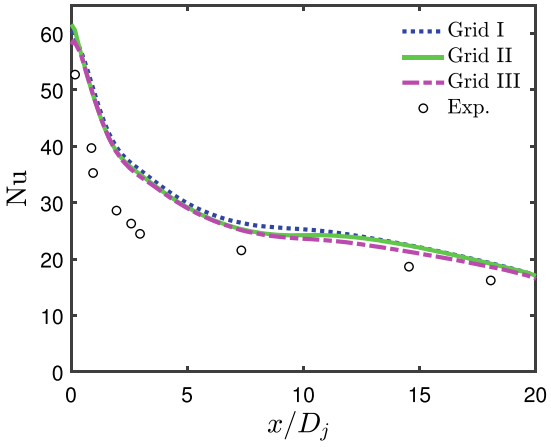


Fig. 3. Nusselt distribution for GEKO solution with varying numerical resolution, compared to experimental data [6].

involving the corner and curvature corrections are neglected. Regardless of tubulence modeling, the value of 0.85 is prescribed for the turbulent Prandtl number.

Table 5. Turbulence models and optional limiters.

Model	Options
Realizable k-ϵ	Production limiter, enhanced wall treatment
k-ω SST	Production Kato–Launder, production limiter
GEKO	Production Kato–Launder, production limiter

In RANS calculations, turbulence production limiters are often needed to prevent excessive turbulence generation in regions with strong streamline curvature, stagnation, or strong strain rates. As such, the influence of Kato-Launder and production limiters on the predicted Nusselt number is also investigated. The different modeling approaches are summarized in Table 5.

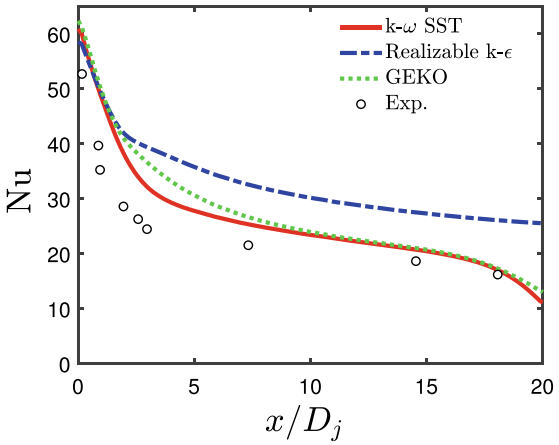


Fig. 4. Nusselt number distribution for different turbulence models without using any limiters, compared to experimental data [6].

Figure 4 shows the Nusselt number distribution along the impingement plate for the three different turbulence models, without using any limiters, compared against experimental measurements [6]. Figure 5 shows the same data obtained by activating both Kato-Launder and production limiters for k-ω SST and GEKO, whereas only the production limiter option is enabled for realizable k-ϵ. From inspection of these pictures, it is possible to observe that all the turbulence models tested follow the general trend of the experimental data, yet with varying degree of accuracy. The k-ω SST and GEKO models show a better

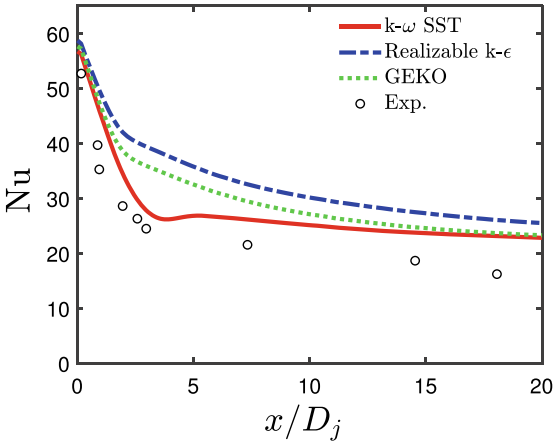


Fig. 5. Nusselt number distribution for different turbulence models with using limiters (see Table 3), compared to experimental data [6].

agreement with the experimental values, particularly in the region close to the stagnation point ($x/D_j < 5$). However, further downstream, these models tend to overpredict heat transfer, especially the realizable k-ϵ model, which shows significant discrepancies throughout the plate surface. This model systematically overestimates the Nusselt number, being unable to correctly predict the turbulence structure and energy dissipation in the impinging jet configuration. When correction limiters are enabled, the agreement with experimental data improves significantly, particularly for the k-ω SST and GEKO models. Apparently, the k-ω SST procedure accurately captures the sharp drop in the Nusselt number in the downstream region, showing the best overall correlation with the experimental findings. However, the GEKO model still overpredicts the Nusselt number distribution along the plate, but shows an improved trend compared to the limiter-free case. Finally, the realizable k-ϵ model continues to struggle in matching the experimental data, indicating that even using limiters, this model does not represent the best choice for predicting heat transfer in impinging slot jets, confirming previous findings [15].

The current results show that the default GEKO parameters are not optimal for heat transfer jet applications. Recently, Yüksekdağ et al. [13] conducted a research on the variations of the GEKO parameters in incompressible round jet impingement. The best agreement with the experimental findings was obtained with the values reported in Table 6, where $C_{nw,sub}$ and $C_{bf,t}$ are two auxiliary parameters. Specifically, $C_{nw,sub}$ is used to modify the log-layer shift to either laminar or turbulent regime, while $C_{bf,t}$ is a parameter linked to the blending function (which is used to deactivate C_{mix} and C_{jet} inside the boundary layer).

The effect of using these additional coefficients is illustrated in Fig. 6, showing the Nusselt number distribution for the two different sets of parameters, with and without using limiters. In both cases, the results of the default GEKO parameters

Table 6. Values of GEKO parameters.

Parameter	Value
C_{sep}	1.1
C_{nw}	2
C_{mix}	–0.7 (constant value)
C_{jet}	0.9
C_{corner}	disabled
C_{curv}	disabled
$C_{nw,sub}$	2.25
$C_{bf,t}$	3.0

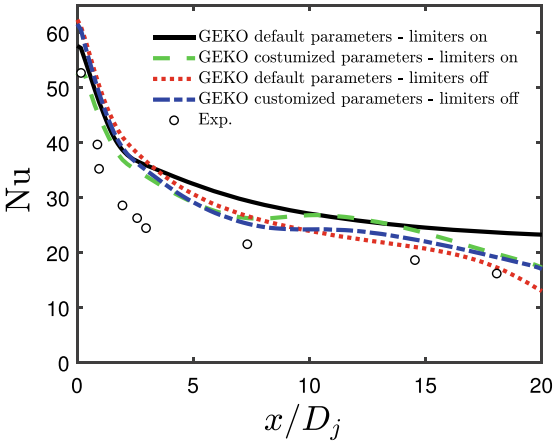


Fig. 6. Nusselt number distribution for different settings of GEKO model parameters with and without using limiters, compared to experimental data [6].

and the newly calibrated GEKO are plotted alongside the experimental values. When considering the Nusselt number peak in the stagnation flow region, the use of customized GEKO parameters and production limiters provides results more aligned with the experiments, suggesting improved predictive performance. However, despite this improvement, both sets of parameters overestimate the Nusselt number in regions further downstream. Basically, as the new GEKO parameters provide a better match to experimental results when limiters are applied, further refinements are however necessary to address overestimation in the outer flow regions.

The pressure distribution along the plate is presented in Fig. 7, normalized by P_0. Making a comparison against reference experimental data [6], the pressure distribution exhibits a maximum value at the stagnation point ($x/D_j = 0$) due to the direct impact of the jet. This peak is followed by a nearly exponential decay as the flow spreads along the wall-parallel direction, aligning with the

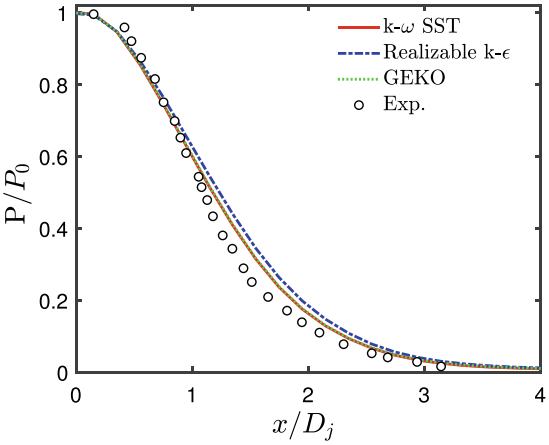


Fig. 7. Normalized pressure distribution over the plate for different turbulence models, compared to experimental data [6].

classical theory of impinging jets [20], as well as experimental findings [24]. This behavior highlights the strong normal pressure gradient in the stagnation region and the subsequent reduction in pressure as the jet transitions into a wall jet. Among the various turbulence models analyzed, the k-ω SST and GEKO models exhibit better agreement against experimental data, particularly near the stagnation point. However, beyond x/D_j=1, deviations from experimental values become more pronounced, particularly for the realizable k-ϵ model, which tends to slightly overestimate the pressure away from the impingement region, due to excessive turbulent diffusion. Minor discrepancies between numerical and experimental data might result from the inherent limitations of RANS turbulence models in accurately capturing unsteady vortical structures along the plate, as observed in [25,26].

Furthermore, the profiles of wall-normal velocity component and velocity magnitude at different locations from the plate are presented in Fig. 8 and Fig. 9, respectively, compared to reference experimental data [5]. Both quantities are normalized using the inlet jet velocity V_j. Importantly, the ability of turbulence models to accurately capture velocity distribution plays a crucial role in predicting heat transfer behavior [27]. All turbulence models appear to provide reasonable predictions of the mean velocity field, particularly at x/D_j=2. However, the k-ω SST and GEKO models demonstrate better agreement with the experiment [5], which also leads to improved predictions of both pressure and Nusselt number. However, the realizable k-ϵ tends to underpredict velocity distributions, causing discrepancies in pressure decay and heat transfer predictions. This suggests that the model struggles to fully capture momentum transfer within the jet, likely due to its limitations in handling highly sheared and recirculating flows. Despite these differences, the overall agreement between numerical and experimental results remains acceptable, demonstrating that all the investigated

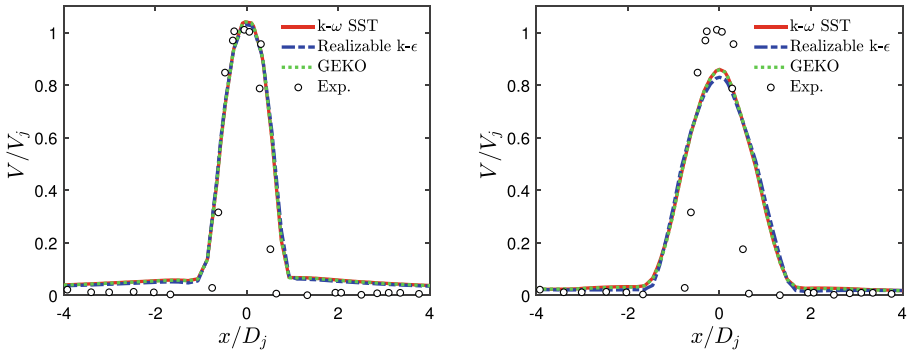


Fig. 8. Profiles of wall-normal velocity component at $y/D_j = 5$ (left) and 2 (right), for different turbulence models, compared against experimental data [5].

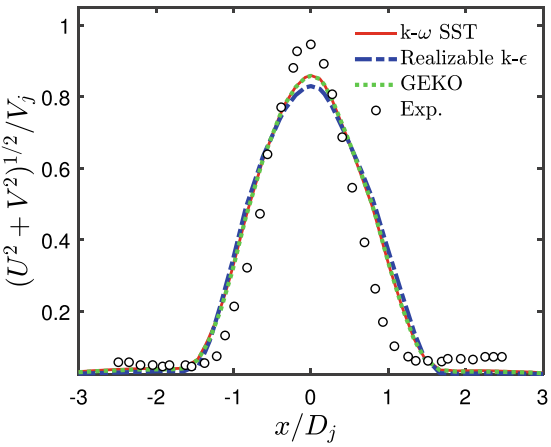


Fig. 9. Profiles of normalized velocity magnitude at $y/D_j = 2$, for different turbulence models, compared against experimental data [5].

turbulence models are generally quite effective in predicting the velocity distribution and spreading characteristics of the impinging jet.

5 Conclusions

This study presents a comparative numerical investigation of heat transfer in a wide slot jet impinging orthogonally on an isothermal flat plate under incompressible flow conditions. Various simulations of the jet cooling process were performed using three RANS-based turbulence models, namely realizable k-ϵ, k-ω SST and the generalized k-ω (GEKO) models. The numerical results were validated against experimental data in terms of Nusselt number distribution, surface pressure profile, and mean velocity fields.

All models accurately captured the pressure peak in the stagnation region, but notable differences emerged in their heat transfer predictions. The realizable k-ϵ model consistently overpredicted the Nusselt number due to excessive turbulent diffusion, making it unsuitable for this particular flow configuration. In contrast, the k-ω SST model showed strong agreement with the experimental data, particularly near the stagnation point. The GEKO model was evaluated either using the default coefficients or employing two alternative sets of parameters. In fact, the default coefficients were found to inadequately represent the physics of the impinging jet flow, leading to an overestimation of the Nusselt number. By modifying key model parameters, including a couple of auxiliary coefficients, which adjust the log-layer behavior and deactivate shear-related terms within the boundary layer, the generalized model achieved substantially better alignment with experimental observations.

Additionally, the implementation of production limiters was shown to improve the accuracy of numerical predictions, particularly in reducing the excessive turbulent kinetic energy generation at the stagnation region, which represents a common limitation in RANS simulations of impinging jets. In summary, while the k-ω SST model performs robustly without calibration, the GEKO model, when suitably tuned, offers enhanced flexibility and potential for accurate heat transfer prediction in jet impingement applications.

Future work will explore the influence of additional parameters on the Nusselt number distribution, assessing the performance of the generalized modeling procedure under diverse flow conditions. Specifically, further investigations will focus on testing the accuracy of the GEKO model in jet flow configurations involving a moving plate and different nozzle-to-plate distances, to evaluate the generalizability of the results and the robustness of the model under dynamic conditions. The analysis will be performed by also exploring more advanced turbulence models, such as detached-eddy simulation (DES), delayed detached-eddy simulation (DDES), and wall-modeled large-eddy simulation (WMLES), e.g. [28–30], where surface roughness effects could possibly be addressed [31].

Acknowledgments. The authors acknowledge financial support under the National Recovery and Resilience Plan (NRRP), Mission 4, Component 2, Investment 1.1, Call for tender No. 104 published on 2.2.2022 by the Italian Ministry of University and Research (MUR), funded by the European Union – NextGenerationEU – Project 2022B2X937 Title "Next Generation Space Propulsion Design Techniques" – CUP E53D23003080006 - Grant Assignment Decree No. 961 adopted on 30.6.2023 by MUR.

Disclosure of Interests. The authors have no competing interests to declare that are relevant to the content of this article.

References

1. Jiang, C., Han, T., Gao, Z., Lee, C.H.: A review of impinging jets during rocket launching. Prog. Aerosp. Sci. **109**, 100547 (2019)
2. Nguyen, T., Maher, B., Hassan, Y.: Flowfield characteristics of a supersonic jet impinging on an inclined surface. AIAA J. **58**, 1240–1254 (2020)

3. Mezzacapo, A., De Stefano, G.: Computational evaluation of turbulent supersonic jet impinging on inclined plate. Appl. Sci. **14**, 7910 (2024)
4. Nakai, Y., Fujimatsu, N., Fujii, K.: Experimental study of underexpanded supersonic jet impingement on an inclined flat plate. AIAA J. **44**, 2691–2699 (2006)
5. Senter, J., Solliec, C.: Flow field analysis of a turbulent slot air jet impinging on a moving flat surface. Int. J. Heat Fluid Flow **28**, 708–719 (2007)
6. Gardon, R., Akfirat, J.C.: The role of turbulence in determining the heat-transfer characteristics of impinging jets. Int. J. Heat Mass Transf. **8**, 1261–1272 (1965)
7. Tsubokura, M., Kobayashi, T., Taniguchi, N., Jones, W.P.: A numerical study on the eddy structures of impinging jets excited at the inlet. Int. J. Heat Fluid Flow **24**, 500–511 (2003)
8. Hattori, H., Nagano, Y.: Direct numerical simulation of turbulent heat transfer in plane impinging jet. Int. J. Heat Fluid Flow **25**, 749–758 (2004)
9. Jaramillo, J.E., Trias, F.X., Gorobets, A., Pérez-Segarra, C.D., Oliva, A.: DNS and RANS modelling of a turbulent plane impinging jet. Int. J. Heat Mass Transfer **55**, 789–801 (2012)
10. Uddin, N., Kee, P., Weigand, B.: Heat transfer by jet impingement: a review of heat transfer correlations and high-fidelity simulations. Appl. Therm. Eng. **257**, 124258 (2024)
11. Bovo, M., Davidson, L.: On the numerical modeling of impinging jets heat transfer - a practical approach. Numer. Heat Transf. A Appl. **64**, 290–316 (2013)
12. Dutta, R., Dewan, A., Srinivasan, B.: Comparison of various integration to wall (ITW) RANS models for predicting turbulent slot jet impingement heat transfer. Int. J. Heat Mass Transf. **65**, 750–764 (2013)
13. Yüksekdağ, R., Koçak, D., Şentürk, U.: Prediction of heat transfer for a single round jet impingement using the GEKO turbulence model. Int. J. Heat Fluid Flow **109**, 109538 (2024)
14. Cademartori, S., Cravero, C., Marini, M., Marsano, D.: CFD simulation of the slot jet impingement heat transfer process and application to a temperature control system for galvanizing line of metal band. Appl. Sci. **11**, 1149 (2021)
15. Gurgul, S., Fornalik-Wajs, E.: On the measure of the heat transfer performance of RANS turbulence models in single round jet impingement. Energies **16**, 7236 (2023)
16. Aghahani, M., Eslami, G., Hadidi, A.: Heat transfer in a turbulent jet impinging on a moving plate considering high plate-to-jet velocity ratios. J. Mech. Sci. Technol. **28**(11), 4509–4516 (2014). https://doi.org/10.1007/s12206-014-1018-1
17. Isman, M.K., Pulat, E., Etemoglu, A.B., Can, M.: Numerical investigation of turbulent impinging jet cooling of a constant heat flux surface. Numer. Heat Transf. A **53**, 1109–1132 (2008)
18. Wilcox, D.C.: Formulation of the k-ω turbulence model revisited. AIAA J. **46**, 2823–2838 (2008)
19. Shih, T.H., Liou, W.W., Shabbir, A., Yang, Z., Zhu, J.: A new k-ϵ eddy viscosity model for high Reynolds number turbulent flows. Comput. Fluids **24**, 227–238 (1995)
20. Pope, S.B.: Turbulent Flows. Cornell University, New York (2000)
21. Menter, F.R., Matyushenko, A., Lechner, R.: Development of a generalized k-ω two-equation turbulence model. Notes Numer. Fluid Mech. Multidisc. Des. **142**, 101–109 (2020)
22. Rossano, V., De Stefano, G.: Testing a generalized two-equation turbulence model for computational aerodynamics of a mid-range aircraft. Appl. Sci. **13**, 11243 (2023)

23. De Stefano, G., Denaro, F.M., Riccardi, G.: Analysis of 3D backward-facing step incompressible flows via a local average-based numerical procedure. Int. J. Numer. Meth. Fluids **28**, 1073–1091 (1998)
24. Li, X., Liu, X., Liu, Y., Peng, D.: Experimental study of near-wall underexpanded jet impingement on a flat plate using temperature-insensitive semi-transparent pressure-sensitive paint. Exp. Fluids **61**(11), 1–17 (2020). https://doi.org/10.1007/s00348-020-03068-5
25. Yadav, H., Agrawal, A.: Effect of vortical structures on velocity and turbulent fields in the near region of an impinging turbulent jet. Phys. Fluids **30**, 035107 (2018)
26. Hadžiabdić, M., Hanjalić, K.: Vortical structures and heat transfer in a round impinging jet. J. Fluid Mech. **596**, 221–260 (2008)
27. Liu, L., Ahmed, U., Chakraborty, N.: A comprehensive evaluation of turbulence models for predicting heat transfer in turbulent channel flow across various Prandtl number regimes. Fluids **9**, (2024)
28. De Stefano, G., Vasilyev, O.V.: Hierarchical adaptive eddy-capturing approach for modeling and simulation of turbulent flows. Fluids **6**, 83 (2021)
29. Ge, X., De Stefano, G., Hussaini, M.Y., Vasilyev, O.V.: Wavelet-based adaptive eddy-resolving methods for modeling and simulation of complex wall-bounded compressible turbulent flows. Fluids **6**, 331 (2021)
30. De Stefano, G., Vasilyev, O.V.: "Perfect" modeling framework for dynamic SGS model testing in large eddy simulation. Theor. Comput. Fluid Dyn. **18**, 27–41 (2004)
31. Salomone, T., Piomelli, U., De Stefano, G.: Wall-modeled and hybrid large-eddy simulations of the flow over roughness strips. Fluids **8**, 10 (2023)